communications biology

A Nature Portfolio journal

Article

https://doi.org/10.1038/s42003-026-09541-x

Widefield cortical activity and functional connectivity during motorized locomotion

Chang Hak Lee[1,3], Gawon Lee[1,3], Hyejin Song[1,3] & Kwang Lee[1,2]

The ability to move within a given environment necessitates constant regulation of sensory and motor functions. However, intricacies of sensory-motor integration via intercortical signal correlation remain to be fully elucidated. In this study, we dissociated internally driven cortical dominance from original signals by removing the influence of behavior variables during locomotion on motorized treadmill, wheel, and disk. There were no significant differences in either original or internally driven activity across the cortex of mice during walking based on the type of track. However, the spatial pattern of internally driven cortical connectivity depended on the track type. Especially, internally driven functional connectivity during sustained locomotion on the treadmill significantly decreased only in the medial M2 regions. Thus, the maintenance of stable locomotion on a linear runway is indicative of successful internal sensory-motor integration, which is achieved through inhibitory control of M2. Our findings demonstrate that the spatial patterns of cortical functional connectivity during locomotion are altered by the gait kinematics following physical rotation of the track. Furthermore, we suggest that understanding of health and disorder related to locomotion in environmental contexts requires the consideration of internally driven activity and functional connectivity across the widefield cortex.

We perceive environmental conditions through the continuous interaction between sensory stimuli and motor actions, and immediate behavioral responses to sudden environmental changes are critical for survival. Sensory information from the body and environment influences the command to form a movement[1–5], and the feedback or feedforward of the movement is integrated with sensory input to maintain locomotion, internally[6–8]. The neural mechanisms underlying locomotion have been extensively studied, with evidence indicating that the projection of signals from the cerebral cortex to subcortical and spinal regions plays a crucial role in regulating movement[9–11]. However, intercortical sensory-motor integration remains unclear. Recently, the secondary motor cortex (M2) has been demonstrated to exhibit interconnectivity with other cortical areas in response to motor-evoked stimuli during voluntary and motorized locomotion[12–15]. Nevertheless, the neural signals underlying movement on curved or spinning ground have yet to provide a comprehensive explanation for the interplay between sensory input and motor output in the context of inherent locomotion.

Here, we used widefield imaging to examine how the spatial interconnection of the entire cortex is influenced by the gait kinematics. Locomotion was performed on three types of motorized tracks: treadmill (flat belt), wheel (round cylinder), and disk (spinning around the central axis). To extract internally driven cortical activity and functional connectivity (FC), the effects of motion-captured behavior variables were removed from the original calcium data using statistical regression. The results indicated an absence of track-dependent variations in cortical activation during walk. However, we found that the spatial patterns of FC in the cerebral cortex significantly depended on locomotion that conformed to the experimental ground environment. Notably, the treadmill, a linear track that promotes relatively stable locomotion, exhibited significantly lower internally driven FC of medial M2 during walking, compared to the wheel or disk track. These results indicate that sensory-motor cortical integration for locomotion is regulated by inhibition of M2. Taken together, we propose that the choice of behavioral models in widefield imaging needs to take into account the kinematics of the body and the corresponding relationship between cortical activity and FC.

Results

Cortical activity independent from the influence of behavior variables in locomotion

To monitor neural activity across the entire cortical area, we performed widefield calcium imaging in Thy1-GCaMP6f mice[16], in which the Thy1 promoter induces GCaMP6 expression primarily in excitatory neurons of cortical layers 2/3 (Fig. 1a). To simulate locomotion state, mice were forced to walk on the motorized treadmill. Head-fixed mice were trained to step

[1]Department of Brain Sciences, Daegu Gyeongbuk Institute of Science & Technology (DGIST), Daegu, Republic of Korea. [2]Center for Synapse Diversity and Specificity, DGIST, Daegu, Republic of Korea. [3]These authors contributed equally: Chang Hak Lee, Gawon Lee, Hyejin Song. e-mail: klee@dgist.ac.kr

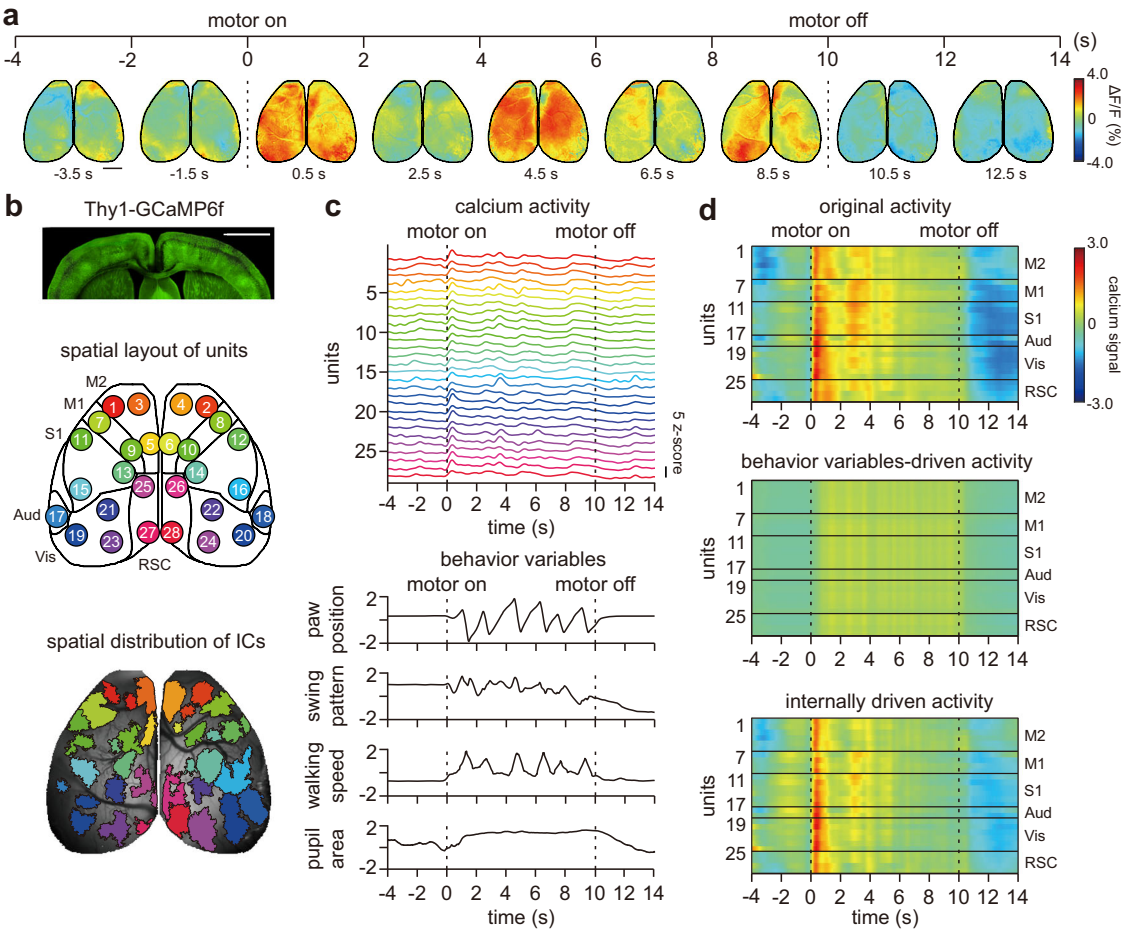

Fig. 1 | Cortical fluorescence imaging after removal of effect of the behavior variables during locomotion. a Schematic of widefield calcium imaging during motorized locomotion. Sequential images of the dorsal cortex were captured during locomotor training on a motorized treadmill (scale bar: 2 mm). The baseline-corrected fluorescence (ΔF/F) exhibited distinct modulation of neural activity throughout the cortex. **b** *top* GCaMP6f expression in the cerebral cortex (scale bar: 2 mm). *middle* Spatial layout of 28 units was consistently observed in all mice and grouped into six cortical regions. *bottom* The spatial distribution of independent components (ICs) is indicative of unit boundaries. Each IC was represented by the same color as the assigned unit ID. The domain range of each IC excluded blood vessel. **c** During a locomotion trial on a motorized treadmill, calcium activity from all cortical units and behavior variables of kinematics—including paw position, swing pattern, walking speed, and pupil area—were measured simultaneously. The standardization of all acquired data to z-scores was performed. **d** The calcium signal in the cerebral cortex of each unit during a motorized locomotion trial was measured both before (*top*) and after (*bottom*) the removal of the influence of behavior variables (*middle*) using PLSR.

forward by placing their paws on a rotating track and facing the opposite direction of rotation. The track was rotated at a speed of 11 mm/s for a duration of 10 s, after which it was halted for a period of rest. Mice were permitted to ambulate or repose immediately following the activation or deactivation of the motorized track. The 3 s following the motor onset was designated as the "start" period for initiation of locomotion, and the 3 s following the motor offset was presented as the "stop" period for termination of locomotion. Steady gait for 3 s after 5 s of motor onset on the motorized track was designated as the "walk" period. Fluorescence of the cerebral cortex was measured through the implanted crystal skull, a curved optical glass that replaced the cranium[17]. Widespread cortical image was captured using a custom-built macroscope with a large field of view. The pixel-wise activity was then represented as a calcium-dependent signal by discarding the hemodynamic artifact of isosbestic fluorescence. Baseline-corrected fluorescence (ΔF/F) exhibited a rapid increase in most areas of the cortex at motor onset, followed by a subsequent immediate decrease. Temporal fluctuations in activity were observed during walk, and cortical activity returned to resting state levels after the motor offset.

To isolate local neural activity, we computed widefield images using spatial independent component analysis (sICA). The sICA, a blind source separation algorithm, identified multivariate signals into subcomponents with statistical independence using the joint approximation and diagonalization of eigenmatrices (JADE)[18]. And spatial domains demonstrating signal contamination arising from vascular fluctuations during movement were manually eliminated. The calcium fluorescence signal in the cerebral cortex was decomposed into independent components (ICs) with functional parcellation of spatial dynamics. The ICs corresponded to the assigned units in the cortical regions and were then aligned with the Allen Mouse Common Coordinate Framework[19]. Next, the 28 units were categorized into six anatomical cortical regions, including the primary motor cortex (M1), secondary motor cortex (M2), primary somatosensory cortex (S1), auditory cortex (Aud), visual cortex (Vis), and retrosplenial cortex (RSC) (Figs. 1b and S1). Subsequently, the data per frame for each unit was calculated by averaging the pixel signal from the mask of the corresponding spatially independent component. Finally, a standardized z-score of the 28 units was extracted from the time-series imaging of sequential frames to reveal clear temporal modulation of neural activity, respectively (Fig. 1c, top). The majority of the cortical modulation over the 28 units exhibited an increase during the "start" and "continuous" locomotion periods, while a decrease was observed during the "stop" locomotion period.

The activity patterns exhibited by each cortical unit involved in locomotion on a motorized treadmill encompass internally driven motor

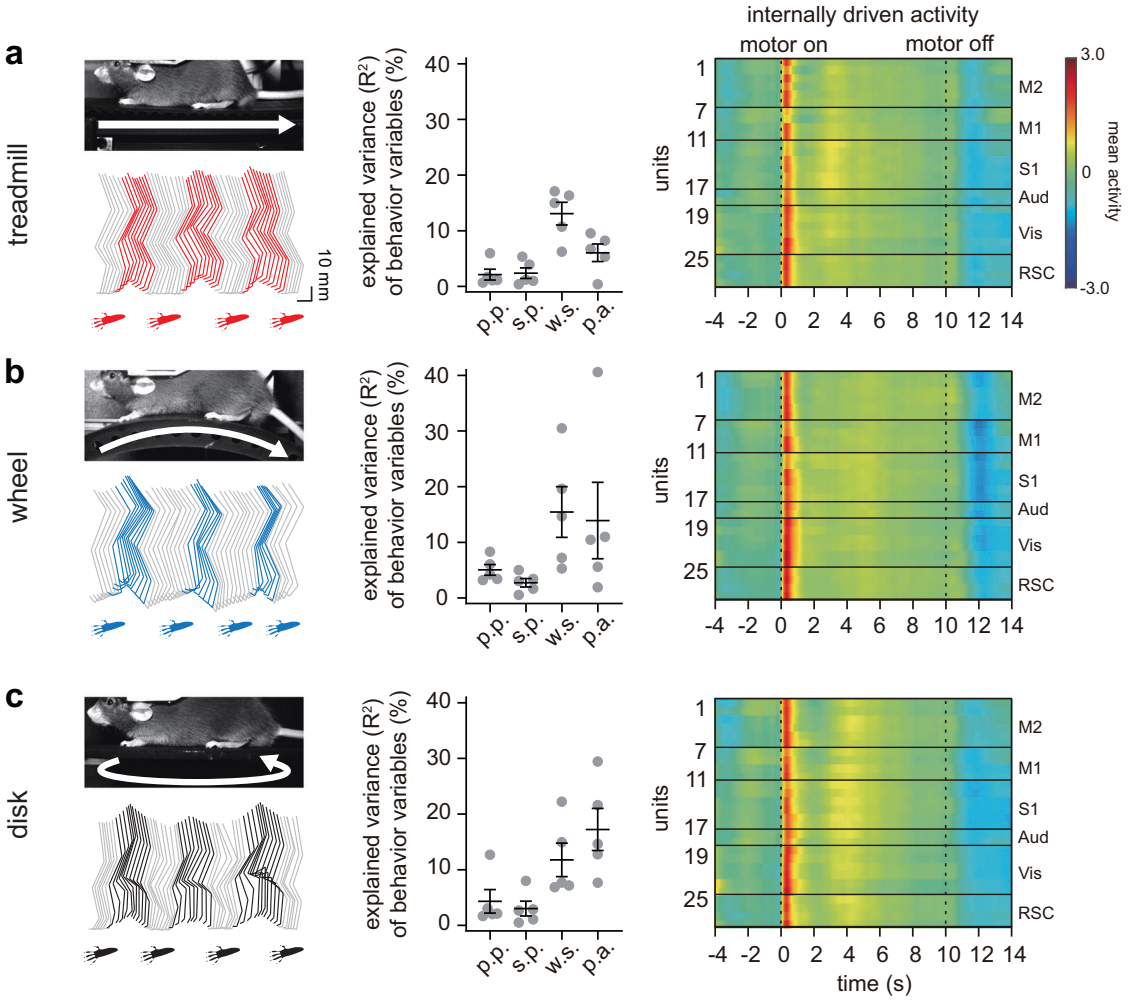

Fig. 2 | The influence of the behavior variables on cortical activation during motorized locomotion. The **a** treadmill, **b** wheel, and **c** disk tracks offered different environments for locomotion. *left* The kinematics trajectory of hindlimb during gait and paw plots indicate individual ground contact. *middle* The influence of paw position (p.p.), swing pattern (s.p.), walk speed (w.s.) and pupil area (p.a.) explained the variance in cortical activation for 10 s after motor onset. Data are expressed as mean ± SEM. *right* The mean calcium activity of each unit after PLSR correction on the motorized treadmill ($n = 5$), wheel ($n = 5$), and disk ($n = 5$) tracks during locomotion of 40 trials.

commands and behavior variables-driven kinematic information. Consequently, a regression analysis was performed to ascertain the contribution of movement, with the relationship between the observed brain signals and the latent variables of behavior being modeled. Behavioral images of the face and body of the mice were recorded concurrently, using dual CMOS cameras positioned parallel to and at a fixed distance from the subjects. And we obtained behavior variables through gait analysis of the hindlimb with pose tracking of mice performing locomotion. We employed markerless motion capture to record six hindlimb joints (toe, metatarsophalangeal joint, ankle, knee, hip, and iliac crest) during gait on the treadmill, and we obtained behavior variables derived from hindlimb kinematics. Subsequently, the behavior variables pertaining to paw position (x dimension), swing pattern (y dimension), gait speed (x and y variation), and pupil area were standardized by *z*-score (Fig. 1c, bottom).

To standardize the impact of the measured behavior variables on cortical activity, we employed a partial least squares regression (PLSR) statistical model. This model utilized the activity of each sICA unit as the dependent variable and four behavior variables as the independent variables. PLSR analysis identified the latent factors underlying the kinematics derived from the behavior variables for each behavioral period (Fig. 1d). The residuals of the regression, calculated as the difference between actual and latent activity, represented the activation independent of the influence of measured behavior variables. Finally, the cortical activity for internally driven locomotion was represented via PLSR correction.

Internally driven cortical activity during motorized locomotion

Three categories of motorized tracks were employed to establish a range of locomotion environments (Figs. 2 left and S2b). The treadmill provided a linear path on flat ground, while the wheel maintained a linear path on cylindrical ground. Conversely, the disk exhibited a nonlinear path characterized by a vertical-axis rotation on a horizontal ground. Mice were trained to ambulate on the designated track when the motor was operated on the treadmill, wheel, or disk track. Behavior variables were obtained by accessing the kinematic trajectory of the hindlimb joints during gait on a track (see Fig. S2c). In the gait analysis, the paw position, swing pattern, and walking speed were contingent on the rotation of the track, which varied for different types of motorized operations. The gait on the treadmill track exhibited smaller step count and longer swing time compared to those gaits on the wheel and disk tracks (Fig. S2d). This finding suggests that the treadmill provides optimal stability for locomotion.

We extracted units of the coordinated cortex region from widefield fluorescence imaging during "walk" period on the motorized tracks. Next, the average cortical activity of each unit was visualized, with differences from rest in each behavioral period. Since there was no difference in activity between the left and right hemispheres in widefield imaging, the activity was presented as the average activity of the left and right side (Fig. S3). In all cases, significant increases in cortical activity were observed with the onset of locomotion during the "start" period following motor operation. The most pronounced activations were observed in M2, followed by M1, S1, and RSC

(Fig. S4a). Locomotion on the wheel track induced the strongest activation in the whole cortex during the "start" period. During the "walk" period, the cortical activity on the treadmill track was comparatively weaker than that of the wheel and disk tracks. However, differences in cortical activity among tracks during continuous locomotion were not statistically significant in all units (Fig. S4b). In the "stop" period following motor offset, the cortical activity on the treadmill track returned to the resting state level. Conversely, the neural response of S1 during the "stop" period on the wheel and disk tracks exhibited a greater reduction than in the others of the cortex.

To determine the influence of the behavior variables from native widefield imaging according to motorized gait, the latent factors of kinematics were calculated using PLSR. Explained variance presented 2.4–17.2% of the variability in cortical activation during locomotion (Fig. 2 middle). The dominance and pattern of variance in cortical activation explained by behavioral variables as independent variables differ depending on track type. This indicated that the influence of behavior variables is highly dependent on the track-based gait. Next, the latent factors, categorized by the types of motorized tracks, represented behavior variables-driven activity, defined as the relative contribution of gait itself to neural activity in cortical regions during behavioral periods (Fig. S5). In the context of wheel-track locomotion, the latent factors of behavior variables in cortical activity exhibited greater dominance across all behavioral periods when compared to those observed on the treadmill and disk tracks. Moreover, enhanced activity was detected in M1 and M2 when compared to other cortical regions during the "start" and "walk" periods (see Figs. S5a, b). Conversely, on the disk track, the impact of cortical activity on kinematics was negligible throughout the behavioral periods. Furthermore, the contribution of cortical activity to behavior variables exhibited a greater increase during the "walk" period compared to other periods, suggesting a heightened engagement of these regions during the execution of treadmill locomotion. The behavior variables exhibited reduced dominance in neural activity during the "stop" period.

The PLSR residuals, calculated by subtracting the latent activity of the behavior variables from the actual cortical activity, indicated internally driven neural responses in the cerebral cortex without affecting the kinematics of locomotion on the motorized tracks (Fig. 2 right). After PLSR correction, the cortical activity of each behavioral period was modified according to locomotion on the motorized tracks. The majority of units exhibiting internally driven cortical activity during locomotion exhibited a marked increase in the "start" period, followed by a decrease in the "walk" period. These units subsequently decreased further below resting state activity levels in the "stop" period (Figs. 3a and S6). The cortical modulation on the treadmill track was comparatively minimal during the behavioral periods. In contrast, during locomotion on the wheel track, internally driven cortical activity increased more than that of the other tracks during the "start" period and was more pronounced in the 5/6 units of M2, 21/22 and 23/24 units of Vis, and the 27/28 unit of RSC (Fig. S6a). In addition, the activity of the 5/6 unit of M2 on the disk track during the "start" period exhibited a significant increase, while the responses during the "walk" period underwent a shift, resulting in an increase in the activity of the 3/4 unit of M2 and the 25/26 unit of RSC after PLSR correction (Fig. S6a). Notably, the dynamics of cortical activity during locomotion on the disk track exhibited a similarity to the neural responses on the disk track prior to PLSR correction. Sudden cessation of movement on the wheel and disk tracks has been observed to induce neural modulation of S1. Although there are alterations in cortical activity in several regions according to track during the "walk" period, statistical differences in internally driven cortical activity after PLSR correction during locomotion on the tracks were not significant in all units (Fig. 3b). In overall, walking on the disk track induced the strongest activity throughout the cortex, in contrast, locomotion on the treadmill track dominated in relatively the small activity in the motor and sensory cortex.

Internally driven cortical FC during motorized locomotion

The FC between regional cortical activities was evaluated. The Pairwise Pearson correlation coefficient (r) was calculated between activity-pairs of each unit in a 1 s window. The correlation value was incorporated in time order by sliding window with a 0.25 s step. The time-series correlation matrices contained a total of 378 unit-by-unit r-pairs, which were averaged for each behavioral period. To ascertain the presence of FC, a subsequent comparison of resting and signal correlation was conducted, resulting in the identification of a substantial discrepancy between r_{signal} and r_{rest} values. This finding serves as an indication of FC, as shown in Fig. 4b.

The original cortical FC was defined by the correlation between activity before PLSR correction for each pair of units (see Fig. S7). On the treadmill track, FC exhibited a marked increase across the entire cortex during all behavioral periods. During the initiation of locomotion on the treadmill track, FC increased globally across the cortex (Fig. S7a). However, the 3/4 unit of M2 and the 9/10 unit of M1 demonstrated reduced FC, and the 5/6 unit of M2 exhibited a negative correlation with other units. The r values between each pair of wheel units were predominantly close to zero, indicating an absence of correlation between the regional neural activities of the cortex. Conversely, the initiation of locomotion on the disk track demonstrated robust FC in the majority of M2 regions, as indicated by the 3/4 unit of M2. The spatial configuration of cortical FC during continuous walking on each motorized track exhibited a resemblance to the initial state of walking (Fig. S7b). During the "stop" period on the treadmill track, significant FC was observed across the entire cortex, including the 3/4 and 5/6 units of M2, which exhibited minimal FC during the initial phase and during continuous walking. Upon cessation of movement along the designated wheel track, the cortical FC of the M1, M2, and S1 regions became evident. And during the observation of motor offset on the disk track, the FC signals of M1 and M2, which were induced during the initiation and continuous locomotion, underwent a decrease (Fig. S7c).

After the elimination of the influence of the kinematics of the locomotion behavior through PLSR correction, the cortical FC of each behavioral period was found to be different from the cortical FC prior to PLSR correction (Figs. 4c and S8). The presence of internally driven cortical FC was observed in all motorized tracks during all behavioral periods. On all three tracks, while locomotion initiation elicited widespread cortical responses in FC during the "start" period, the abrupt cessation of movement is indicative of elevated cortical FC during the "stop" period (Fig. S8). During the "walk" period, the apparent spatial correlation between each unit and other regions showed variability depending on the track type (Fig. 4c). The results indicated that continuous walking in all tracks increased overall cortical FC. On the other hand, the FC for locomotion on the treadmill track was relatively more pronounced than that of the wheel and disk task during the "walk" period; a negative correlation was observed in the 5/6 unit of M2. Spatially paired connectivity sets of 1/2, 3/4, 5/6 units in M2, 11/12 and 15/16 units in S1, 17/18 unit in auditory cortex, 21/22 and 23/24 units in visual cortex units, 25/26 and 27/28 units of the RSC were influenced significantly by the track with unique physical rotational mechanisms (Fig. 4d, e). And track-specific dominant or subordinate connectivity units existed; In M2, 1/2 and 3/4 units showed the strongest connectivity on the disk, while 5/6 unit exhibited relatively the weakest connectivity on the treadmill. 15/16 unit of S1 showed the weakest connectivity on the wheel. And 23/24 unit of visual cortex and 25/26 unit of RSC exhibited the strongest connectivity on the disk. Moreover, the weakest connectivity in 27/28 unit of RSC on the wheel was expressed. Thus, the spatial patterns of internally driven FC depend on locomotion on motorized tracks.

The relationship between cortical activity and FC after PLSR correction

We calculated a relationship to determine the similar direction and strength between internally driven cortical activity and FC after PLSR correction. The relationship between these variables can be expressed as the dot product between the normalized activity and FC vectors, as measured by cosine similarity. During the designated "walk" period, the relationship between cortical activity and FC revealed spatial modulation patterns of the cortex for locomotion on three types of motorized tracks (Fig. 5). The relationship between cortical activity and FC during continuous locomotion on wheel and disk tracks showed strong positive values across all units of the cortex-

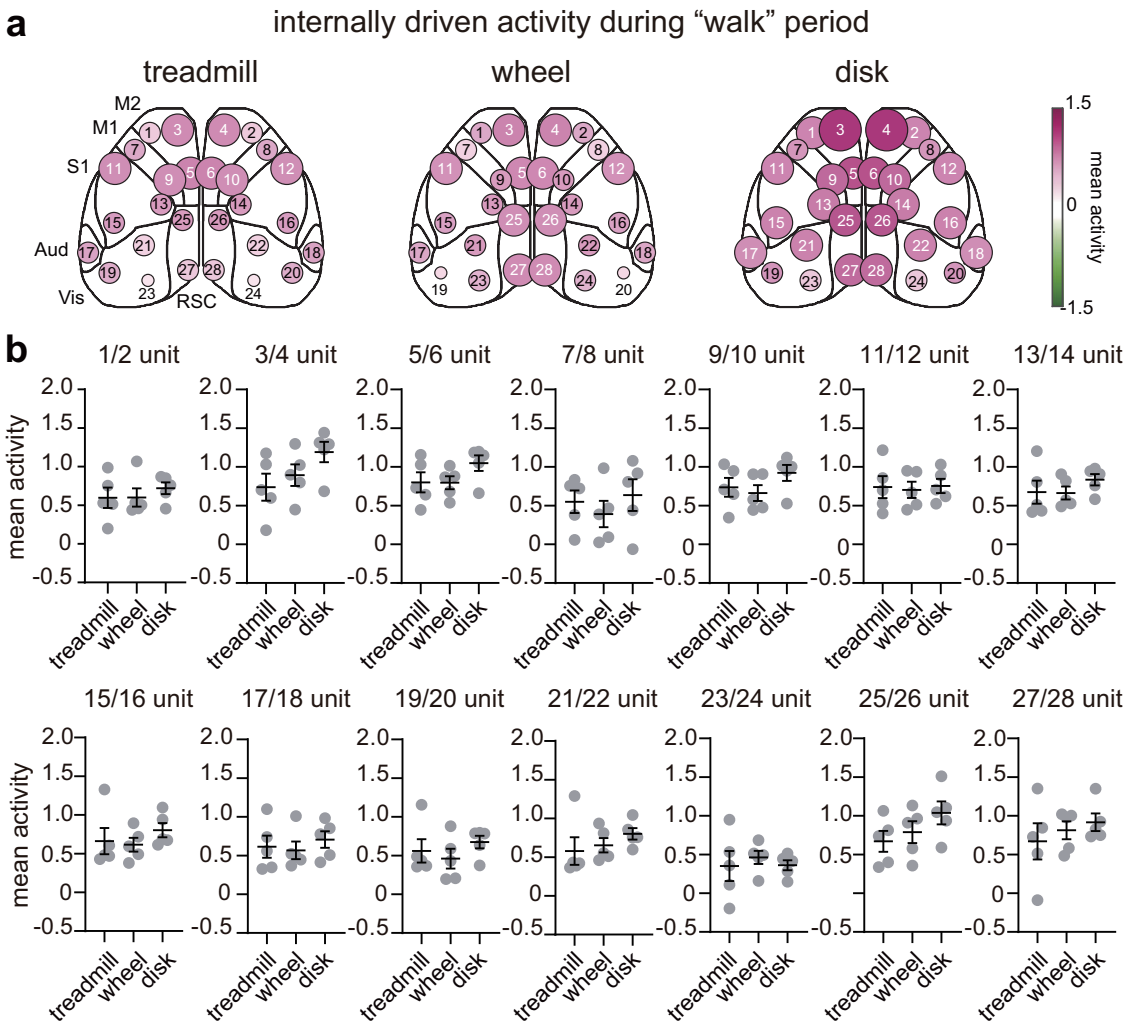

Fig. 3 | Internally driven cortical activity during "walk" period on motorized tracks. a After the removal of the effect of behavior variables on the "walk" period per track, cortical activity was calculated for motorized treadmill ($n = 5$), wheel ($n = 5$) and disk ($n = 5$). In schematic of cortical activity after PLSR correction, the mean internally driven cortical activity of each unit was presented as the difference in resting activity, and only significant changes were shown (paired sample t-test: Benjamini–Hochberg corrected, $p < 0.05$). The circle size and color of each unit represented the amplitude of activity. **b** There was no difference in activity after PLSR correction among tracks in 1/2 unit (one-way RM ANOVA, $F_{2,12} = 0.3994$, $p = 0.6793$), 3/4 unit (one-way RM ANOVA, $F_{2,12} = 2.377$, $p = 0.1350$), 5/6 unit (one-way RM ANOVA, $F_{2,12} = 1.857$, $p = 0.1982$), 7/8 unit (one-way RM ANOVA, $F_{2,12} = 0.5042$, $p = 0.6162$), 9/10 unit (one-way RM ANOVA, $F_{2,12} = 1.506$, $p = 0.2609$), 11/12 unit (one-way RM ANOVA, $F_{2,12} = 0.05239$, $p = 0.9492$), 13/14 unit (one-way RM ANOVA, $F_{2,12} = 0.8029$, $p = 0.4707$), 15/16 unit (one-way RM ANOVA, $F_{2,12} = 0.6349$, $p = 0.5469$), 17/18 unit (one-way RM ANOVA, $F_{2,12} = 0.3345$, $p = 0.7222$), 19/20 unit (one-way RM ANOVA, $F_{2,12} = 0.7598$, $p = 0.4890$), 21/22 unit (one-way RM ANOVA, $F_{2,12} = 0.8387$, $p = 0.4561$), 23/24 unit (one-way RM ANOVA, $F_{2,12} = 0.2336$, $p = 0.7952$), 25/26 unit (one-way RM ANOVA, $F_{2,12} = 1.752$, $p = 0.0.2149$), 27/28 unit (one-way RM ANOVA, $F_{2,12} = 0.5671$, $p = 0.5816$). Data are expressed as mean ± SEM.

wide area without spatial differentiation. And relationship between cortical activity and FC during locomotion on the treadmill exhibited a positive value in the majority of sensory and motor cortices, On the other hand, a negative value was observed in the medial region, 5/6 units of M2.

Discussion

Spatial patterns of cortical activity on locomotor kinematics

Locomotion is defined as the behavioral outcome of signal processing across multiple regions of the cerebral cortex, mediated by sensory-motor integration. Most locomotion studies have examined cortical activity during the "start" or "walk" phases of gait without clearly distinguishing between them[20–22]. More recently, in head-fixed mice, the initial walking state was distinguished from the steady walking state[23], and cortex-wide activation was shown to increase during the first three seconds of both spontaneous and motorized starts[16]. In the present study, we similarly observed cortex-wide activity during the "start" period (Figs. S4a and S9a) and distinguished it from the "walk" period.

PLSR was employed to compute the predicted neural activity derived from the feature extraction of the behavior variables. These variables included kinematics, paw position, swing pattern, and walking speed obtained through gait analysis. Sensory modulation was known to be coupled with gait cycles during forced locomotion on motorized tracks[14]. Pupil area, an externally observable index, was included as an additional behavioral variable because fluctuations in pupil size coincide with locomotion, showing dilation and constrictions upon movement onset and offset, respectively[24], and are tightly linked to locomotion arousal[25,26]. Therefore, the residual activity obtained by subtracting behavioral variable-driven activity from the original widefield calcium signal using PLSR correction reflected internally driven cortical activity during motorized locomotion.

Prior to PLSR correction, locomotion on the wheel track produced the most pronounced cortical activity in the original calcium signals (Fig. S4a). However, after PLSR correction, locomotion during the "walk" state on the disk track exhibited the most prominent activity across extensive regions of the dorsal cortex compared with the other tracks (Fig. S9c).

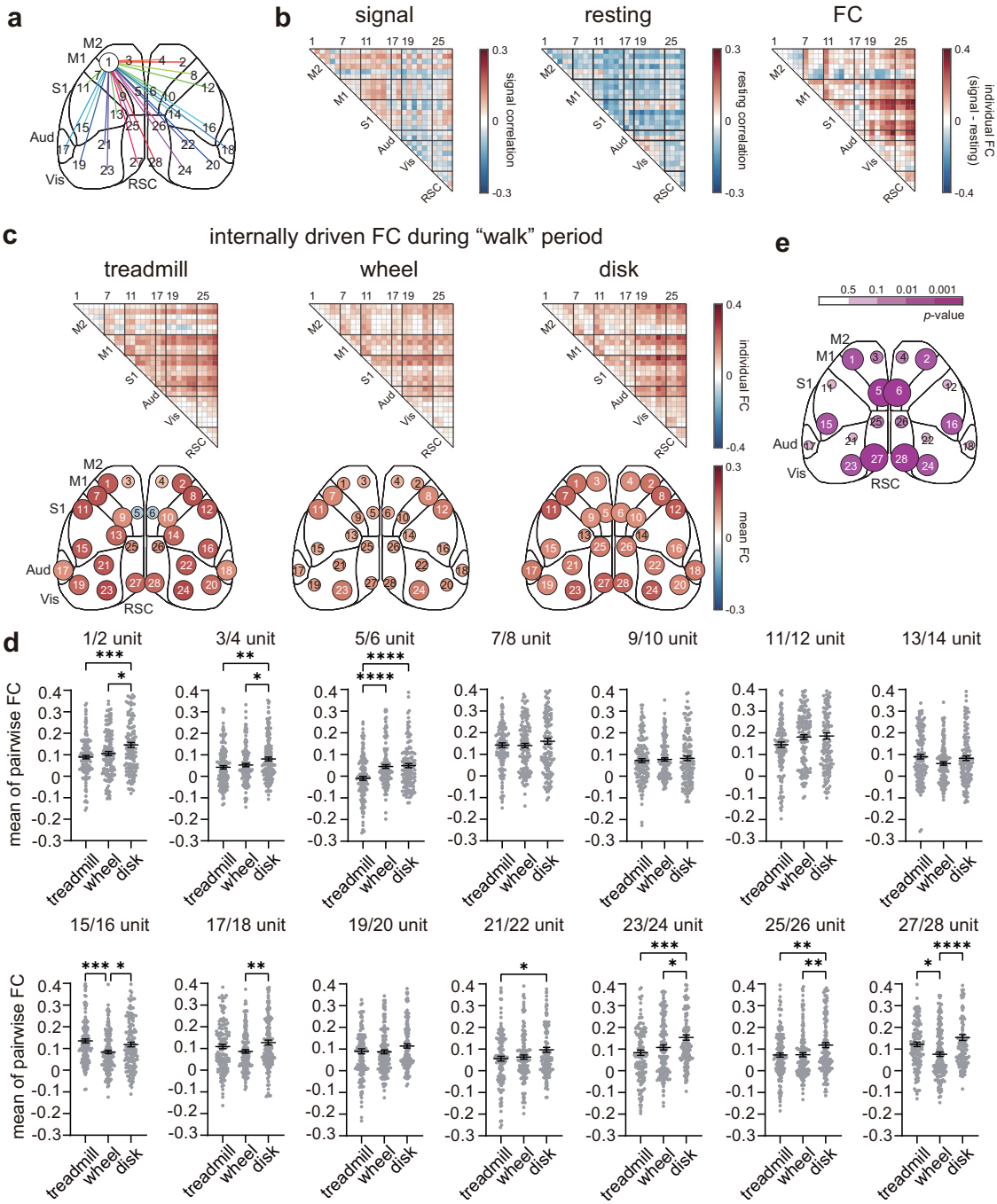

The fractional changes in cortical activity after PLSR correction across tracks are attributable to the latent activity associated with behavioral variables, which was strongest during locomotion on the wheel and least pronounced on the disk (Figs. S5 and S9d). The results of this study demonstrated that 3/4 unit of M2 were dominant in the internally driven cortical activity on the disk track. This finding indicated that locomotion along a nonlinear path characterized by vertical-axis rotation is modulated by internally generated motor commands (Fig. 3a and S6)[8,27]. On the same linear path, the treadmill and wheel exhibited similar spatial patterns of internally driven cortical activity. However, despite sharing a similar linear path, locomotion on the wheel on a cylindrical ground produced stronger variable-driven cortical activity than locomotion on the treadmill on flat ground. During continuous locomotion, the wheel evoked stronger activity in 27/28 unit of the RSC region compared with the treadmill (Fig. 3a). Previous studies have shown that the RSC integrates a variety of sensory inputs, including vestibular signals, to support spatial cognition[21,28–30]. Consequently, during locomotion, the cylindrical ground of the wheel requires a greater degree of internally driven activity than the flat ground to facilitate spatial perception. Overall, the spatial pattern of regional dominance in internally driven cortical activity during motorized locomotion depends on the physical rotation of the track. Nevertheless, no cortical regions showed significant differences in internally driven activity between tracks.

Spatial patterns of cortical FC on locomotor kinematics

Cortical regions can be directly or indirectly correlated with other cortical regions through other brain regions[31,32]. The FC was defined by measuring the similarity between activities arising from two regions. After PLSR correction, cortical FC was exhibited in all cortical regions across all tracks for locomotion during the "walk" period (Fig. 4c) and, the spatial patterns

Fig. 4 | Internally driven functional connectivity (FC) during "walk" period on motorized tracks. a The signal pair connectivity between each original activity of 28 units was calculated using the pairwise Pearson correlation. **b** Signal correlation (r_{signal}, *left*) and resting correlation (r_{rest}, *middle*) matrix for mean cortical activity during locomotion. Time-series correlation data were calculated by sliding windows between activity-pairs of each unit from one animal. Cortical connectivity was computed to compare between signal correlation and resting correlation for each behavioral period ($r_{signal} - r_{rest}$, *right*). **c** The mean change in internally driven cortical FC of unit-pairs was computed for the "walk" periods per track following PLSR correction. Connectivity matrices showed a mean change in the correlation of original signals from the correlation of rest. In schematic of cortical FC, significant change in FC compared to the resting state (paired sample *t*-test: Benjamini–Hochberg corrected, $p < 0.05$) for treadmill ($n = 5$), wheel ($n = 5$) and disk ($n = 5$) with 378 unit-pairs. The circle size and color of each unit represented the FC value. **d** The mean of the whole pairwise FC (n x m; $n = 5$ mice, $m = 27$ connectivity) with spatially paired connections in the left and right hemispheres are presented. The internally driven FC in during locomotion differed significantly across the tracks in 1/2 unit (one-way RM ANOVA, $F_{2402} = 8.835$, $p = 0.0002$, Post-hoc Tukey's multiple comparison: treadmill versus disk, $p = 0.0002$; wheel versus disk, $p = 0.0115$), 3/4 unit (one-way RM ANOVA, $F_{2402} = 6.042$, $p = 0.0026$, Post-hoc Tukey's multiple comparison: treadmill versus disk, $p = 0.0025$; wheel versus disk, $p = 0.0371$), 5/6 (one-way RM ANOVA, $F_{2402} = 13.10$, $p < 0.0001$, Post-hoc Tukey's multiple comparison: treadmill versus wheel, $p < 0.0001$; treadmill versus disk, $p < 0.0001$) of M2. There was no difference in internally driven FC among tracks in 7/8 unit (one-way RM ANOVA, $F_{2402} = 0.9047$, $p = 0.4055$), 9/10 unit (one-way RM ANOVA, $F_{2402} = 0.3263$, $p = 0.7218$) of M1. The internally driven FC in 11/12 unit during locomotion differed across the tracks (one-way RM ANOVA, $F_{2402} = 3.042$, $p = 0.0488$). There was no difference in internally driven FC among tracks in 13/14 unit (one-way RM ANOVA, $F_{2402} = 2.961$, $p = 0.0529$). The internally driven FC in during locomotion differed significantly across the tracks in 15/16 unit (one-way RM ANOVA, $F_{2402} = 8.033$, $p = 0.0004$, Post-hoc Tukey's multiple comparison: treadmill versus wheel, $p = 0.0003$; wheel versus disk, $p = 0.0234$), 17/18 unit (one-way RM ANOVA, $F_{2402} = 4.356$, $p = 0.0134$, Post-hoc Tukey's multiple comparison: wheel versus disk, $p = 0.0095$). There was no difference in internally driven FC among tracks in 19/20 unit (one-way RM ANOVA, $F_{2402} = 2.2$, $p = 0.1121$). The internally driven FC during locomotion differed significantly across the tracks in 21/22 unit (one-way RM ANOVA, $F_{2402} = 4.142$, $p = 0.0166$, Post-hoc Tukey's multiple comparison: treadmill versus disk, $p = 0.0195$). The internally driven FC in during locomotion differed significantly across the tracks in 23/24 unit (one-way RM ANOVA, $F_{2402} = 8.753$, $p = 0.0002$, Post-hoc Tukey's multiple comparison: treadmill versus disk, $p = 0.001$; wheel versus disk, $p = 0.0207$) and 25/26 unit (one-way RM ANOVA, $F_{2402} = 6.294$, $p = 0.002$, Post-hoc Tukey's multiple comparison: treadmill versus disk, $p = 0.0058$; wheel versus disk, $p = 0.0071$), 27/28 unit (one-way RM ANOVA, $F_{2402} = 11.8$, $p < 0.0001$, Post-hoc Tukey's multiple comparison: treadmill versus wheel, $p = 0.0122$; wheel versus disk, $p < 0.0001$) of RSC. $^{*}p < 0.05$, $^{**}p < 0.01$, $^{***}p < 0.001$, $^{****}p < 0.0001$ **e** In schematic of cortical FC, the *p*-value of each unit which differences internally driven FC across tracks was represented. Internally driven FC in all regions of M2 and RSC was influenced by the track. And internally driven FC was affected by the track only in localized S1, the auditory and visual cortex.

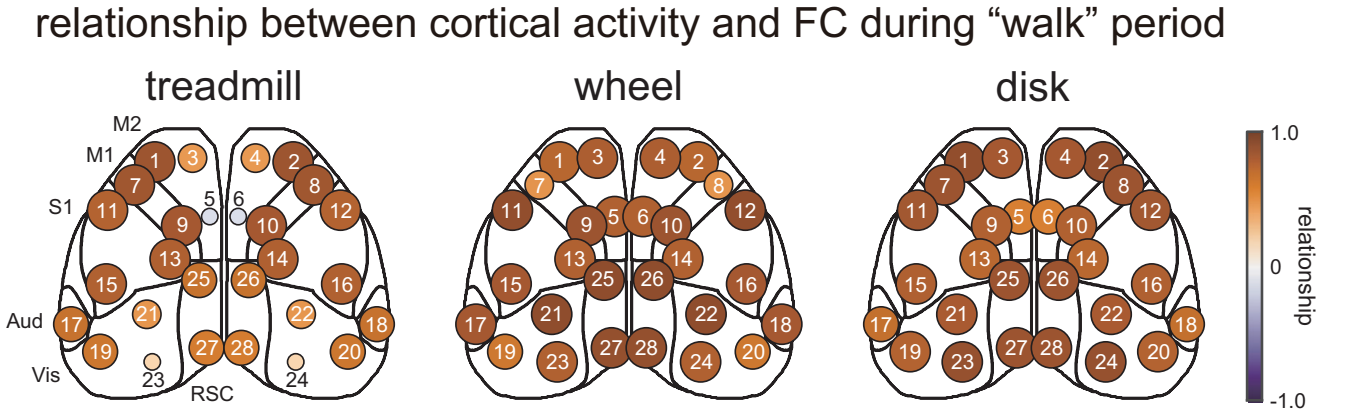

Fig. 5 | The mean relationship between cortical activity and FC of each unit for the "walk" periods was shown after the PLSR correction. The relationship was determined through the calculation of the cosine similarity between the activity vector and the FC vector of individual animals for treadmill ($n = 5$), wheel ($n = 5$) and disk ($n = 5$) during locomotion of 40 trials.

presenting regional dominance of FC differed significantly depending on the specific type of locomotion (Fig. 4d, e). The disk showed stronger FC than the other tracks in the 1/2 and 3/4 units of M2, the 23/24 unit of the visual cortex, and the 25/26 unit of the RSC. This implies that maintaining locomotion on a rotational track requires signal correlation across broader cortical areas. In contrast, the wheel showed relatively lower FC than the other tracks in the 15/16 unit of S1 and the 24/28 unit of the RSC. This indicates that maintaining locomotion on a cylindrical surface requires relatively less connective influence between these areas and other brain regions. Analysis of locomotion patterns on the treadmill revealed a distinct regional pattern of cortical FC compared with the other tracks. Notably, the 5/6 unit of M2 exhibited negative correlations with other units during treadmill locomotion. The medial M2, located in the 3/4 and 5/6 units, exhibits robust limbic FC that facilitates goal-directed movement, motivation, and decision-making processes[33,34]. Recent imaging studies have revealed that cortical FC in response to motor-evoked stimuli is typically dominated by strong M2 dominance[14,35–38]. During relatively steady locomotion on the treadmill, however, the spatial M2 pattern of internally driven FC indicated a stronger association with motor control rather than motor planning.

Spatial patterns of relationship between cortical activity and FC on locomotor kinematics

High-amplitude local activity induces co-fluctuations in activity in other regions[39]. Therefore, to understand the neural responses underlying sensory-motor integration, it is essential to analyze cortical activity and FC within identical brain regions. We hypothesized that the spatial patterns of the relationship between cortical activity and FC after PLSR correction would serve as a map of the overall internal state of the cerebral cortex (Fig. 5). Regarding this relationship, medial M2 executes intercortical inhibition, whereby sensory information is transformed into movement output for continuous locomotion on a motorized treadmill[27,33,40]. The M2 is involved in executing and controlling behavior and in sending efference copies of motor commands to sensory cortical areas[41,42]. Our results showed that locomotion on the motorized wheel and disk required continuous postural adjustments during the "walk" period. This irregular motor control positively highlighted both activity and FC across the global cortex during behavior. In contrast, locomotion on the motorized flat treadmill did not require the transmission of motor control signals from M2 because there were no environmental changes during the "walk" period. The selective suppression of connectivity between a specific cortical region and other

cortical regions implies functional segregation of that area[43,44]. Consequently, M2 activity showed positive values on the treadmill, whereas FC exhibited negative values, indicating an inverse directionality in the relationship between activity and FC. These findings suggest that cortical network reconfiguration—through spatial integration and segregation—differs based on the locomotion context.

When we start or stop walking, the cerebral cortex performs rapid signal processing. The results of this study suggest that the relationship between cortical activity and FC after PLSR during the "start" and "stop" periods represents a transient alteration in sensory-motor integration (Fig. S10). During the "start" period, all tracks produced a sudden positive increase in both activity and FC across the cortex. In contrast, during the "stop" period, most cortical regions exhibited negative activity; however, cortical activity resulted in positive connections with other regions. Consequently, the relationship between cortical activity and FC during the "stop" period showed negative values in most cortical regions on all tracks. These findings are concordant with those of previous studies examining cortical activity and connectivity at the initiation and termination of both forced and voluntary locomotion[14].

Limitations of this study

The primary methodology employed in this study involved discerning the internally driven cortical response to locomotion resulting from the rotation of the track. To this end, PLSR correction was applied to remove intrinsic motion signals from the original spatial components of the cerebral cortex. Although PLSR effectively mitigated the influence of primary behavioral variables on locomotor kinematics, fully eliminating behavior-variable-driven signals remained challenging. In particular, unidentified behavioral variables—such as whiskers, nose, forelimb, tail, and even contralateral hind limb movements, which are not elements of traditional gait analysis—persisted. In the context of non-linear kinematics, such as that of a disk with a vertical axis of rotation, incorporating an additional top view through behavioral imaging is recommended for capturing behavioral variables with greater precision. The potential influence of posture and balance on locomotion also remains a topic of interest for future investigations. Factors disrupting normal locomotion, such as the rotational curvature radius of the track, and high motorization speeds, which make it difficult for the body to react, represent key factors for examining wide-field cortical responses to posture and balance in future studies.

Conclusion

A comparative analysis was conducted on three distinct types of motorized tracks to evaluate cortical responses during locomotion. Locomotion on linear tracks provided a relatively stable environment, suggesting their suitability for investigating internally driven cortical responses. We demonstrated that gait dependent on physical rotational mechanisms of the track does not affect cortical activity patterns but does influence spatial FC patterns. Therefore, our findings indicate that kinematics is a key factor in selecting an appropriate locomotion model. Furthermore, we suggest that wide-field calcium imaging be interpreted comprehensively from the combined perspective of cortical activity and FC.

Methods

Animals

All experimental procedures were approved by the Institutional Animal Care and Use Committee of the Daegu Gyeongbuk Institute of Science and Technology (DGIST-IACUC-21112512-0000 and DGIST-IACUC-24100409-0000). We have complied with all relevant ethical regulations for animal use. For experiments involving widefield imaging of the cerebral cortex for behavioral testing, male transgenic mice (C57BL/6J-Tg(Thy1-GCaMP6f)GP5.17Dkim/J, #025393, The Jackson Laboratory)[16], were used. Transgenic mice were maintained as hemizygous in a C57BL/6J background (#000664, The Jackson Laboratory). Animals were 10–14 weeks old at the time of the surgery. Animals were maintained on a 12 h light cycle, and the group housed until the surgery.

Surgical procedures

Animals underwent surgical procedures under aseptic conditions and isoflurane anesthesia (4% for induction and 1–2% during surgery) on a computer numerically controlled (CNC) machine, Craniobot, for automated craniotomies[45]. The objective of the study was to replace the skull with a curved optical glass of trapezoidal shape, with dimensions of 8 × 10 mm, with a thickness of 0.2 mm and a curvature radius of 10 mm (D263T, Schott)[17]. This replacement was achieved through a large craniotomy over the entire dorsal cortex. The surface profiler of Craniobot (Tormach, SPU-40) contacted with the cranial surface along a predefined trajectory that was slightly smaller than the circumference of the curved optical glass and measured the z-coordinates at several points though the designed craniotomy path. After substitution of the 1 mm diameter mill in the Craniobot, a shallow groove was created along the measured coordinates of the trapezoid. The initial milling depth was set at 30 μm, and the depth was subsequently increased in 10 μm steps until the dura was exposed. The removal of the skull was executed with the aid of surgical forceps, meticulously ensuring the preservation of the dura over the entirety of the exposed brain. Prior to implantation, the curved optical glass was sterilized by soaking in 70% ethanol for 2–3 min, followed by rinsing in sterile saline. The glass was then placed on the exposed brain and aligned with the craniotomy. Dental cement (S380, C&B Metabond, Parkell Inc.) was applied to the periphery of the cranial window, thereby adhering it to the cranial surface. Furthermore, an outer wall was constructed with black dental cement (Ortho-Jet, Lang Dental) along the lateral edge of the cranial window, and stainless-steel head fixation bars were attached to the cerebellar skull. After the surgical procedure, the animals were individually housed and administered daily subcutaneous carprofen injections (5 mg/kg) for the initial three post-operative days. During the first post-operative week, the animals received ibuprofen and amoxicillin, dissolved in their drinking water. Mice were allowed a recovery period of at least 1 week before locomotor training.

Immunohistochemistry

Mice were anesthetized and transcardially perfused with 24 °C phosphate-buffered saline (pH 7.3) and ice-cold paraformaldehyde. Brains were placed in paraformaldehyde overnight, and 100 μm coronal sections were cut with a vibratome. Sections were blocked with normal serum and then incubated overnight at 4 °C with chicken anti-GFP (Abcam, ab13970) as primary antibody (1:1000 dilution). After three washes with PBS, the sections were incubated at 4 °C with Alexa Fluor 488-conjugated donkey antibody to chicken IgG (Jackson ImmunoResearch, 703-545-155) as secondary antibody (1:200 dilution) for 4 h. Sections were mounted with tissue mounting medium and were imaged under epifluorescence microscopy.

Locomotion training

The animals were habituated to head fixation on a motorized track. Three types of tracks were utilized in this study: treadmill, wheel, and disk (see Fig. S2b). We fabricated a custom-designed treadmill and disk (https://github.com/lch199912/TreadmillWidefield). The wheel was modified from the Kinemouse wheel[46]. The tracks under consideration all consisted of a stepper motor (NEMA 17 bipolar stepper motor, Pololu) and gears. The identical rotation speed of the tracks was verified using an encoder (E6B2-CWZ6C, Omron). Furthermore, a rubber spray (Plasti Dip) was applied to the surface of the track to prevent animals from slipping on the rotating track. The mice were head-fixed on the track once a day for approximately 30 min. In the initial training phase, the head position was occasionally adjusted to encourage locomotion, with the head positioned more anteriorly or posteriorly. The head position was then adjusted incrementally, with an average adjustment of 1–2 millimeters per day, until all mice reached the same standard position. During operation of the motor, the tracks were rotated at a velocity of 11 mm/s for 10 s duration. Thereafter, the motor was deactivated. The mice were trained to traverse a rotating track for a period of at least eight days, with an inter-trial interval (ITI) ranging from 20 to 30 s and 40 trials administered daily. The "start" period was defined as the initiation of locomotion during the first 3 s after motor onset. The "walk"

period was defined as steady locomotion during the next 3 s after 5 s of motor onset. The "stop" period was defined as the termination of locomotion during the 3 s after motor offset. Each track was subjected to a group of five mice, and the mice in one cohort did not participate in other cohorts. Mice that were unable to ambulate on the track were excluded from all experiments (approximately 16% of mice). The implementation of custom LabVIEW code (v.2020) was instrumental in triggering motorized locomotion and in the concurrent monitoring of gait and facial behavior using dual cameras (DMK 33UX273, The Imaging Source).

Behavior analysis

Body and face movements were recorded at a rate of 40 frames per second for a duration of 20 s, encompassing a 5 s period before and after locomotion. Six anatomical landmarks of hindlimb kinematics[47], including the toe, metatarsophalangeal joint, ankle, knee, hip, and iliac crest, were tracked using DeepLabCut for markerless pose estimation[48]. The dimensions of the hindlimb and the pupil were determined through a meticulous adjustment of the pixel-based scale, with the known size of the headbar serving as a reference point. A hindlimb step is defined as a movement consisting of two distinct phases: a stance phase and a swing phase. The stance phase was defined as the period during which the paw was in contact with the ground, while the swing phase was defined as the period during which the paw was not in contact with the ground. The position of the paw in contact with the track and the swing pattern of the hindlimb were calculated from the modulation of the toe x-coordinates. The step cycles were counted from the intersection of ankle and hip coordinates. The walking speed was determined by measuring the displacement of the toe *x*- and *y*-axis coordinates across successive frames, with the calculation divided by the frame rate. The modulation of pupil size during locomotion was analyzed using Facemap for orofacial tracking[49]. The area of interest (ROI) of the pupil was extracted from the facial image and quantified in pixel × pixel units for each frame. All analyses of gait and pupil were performed using custom MATLAB scripts (version 9.13 R2022b, MathWorks).

Widefield imaging

Widefield calcium imaging was performed with a custom-built macroscope, equipped with a 0.5 NA macro-objective (MVPLAPO 2XC, Olympus), using an sCMOS camera (Dhyana 95 V2, Tucsen) through the implanted optical glass on the dorsal cortex. The frames were recorded in 16-bit grayscale format without spatial binning using Mosaic 1.6 software (Tucsen) at a frame rate of 40 Hz with an effective resolution of 880 × 880 pixels. The macroscope was composed of two cages: an excitation cage for the light collimation module and a main cage for the objective module. A blue LED (470 nm, M470L4, Thorlabs) and a violet LED (405 nm, M405L4, Thorlabs) were connected to a 30 mm cage cube (C4W, Thorlabs), which contained a 470 nm bandpass filter (65–144, Edmund optics), a 405 nm bandpass filter (65–133, Edmund optics), and a dichroic mirror (69–898, Edmund optics). The excitation light collimated with an adjustable collimator lens (SM2E, Thorlabs). The excitation light paths were merged and then reflected onto the brain surface via a 60 mm main cage cube. Subsequently, the GCaMP6f fluorescence signals traversed a dichroic mirror (T495LPXR-UF2, 50.8 mm × 72 mm, Chroma) and a 520 nm emission filter (ET520/40 m, Ø50 mm, Chroma). Thereafter, the signals were introduced into sCMOS through a tube lens (Ai Nikkor 50 mm f/1.2, Nikon). Alternating 405 nm and 470 nm LED illumination from frame to frame generated a set of frames with violet and blue excitation at a frame rate of 20 Hz. After subtracting the isosbestic fluorescence of violet excitation frames, which include non-calcium-dependent artifacts such as hemodynamics and autofluorescence, from the blue excitation frames, the calcium-dependent signals were recalculated as baseline-corrected fluorescence (ΔF/F) using custom LabVIEW code (v.2020).

Imaging process and sICA

Widefield calcium image analysis was performed using MATLAB scripts. The frames were spatially downsampled to 440 × 440 pixels. For each frame, the MATLAB functions "*imwarp*", "*imregtform*", and "*dftregistration*" were used to generate a geometric transformation matrix, align to the image region, and perform motion correction, respectively. Next, the Allen Mouse Common Coordinate Framework version 3 (CCF) was implemented on the entire set of cortex images. The preprocessed matrix was compressed into projection matrix using singular value decomposition (SVD). The data were represented within the first 200 singular values using a randomized algorithm and were used as input for spatial independent component analysis (sICA). The Joint Approximate Diagonalization of Eigenmatrices (JADE) algorithm was employed to compute 100 independent components (ICs). Subsequently, a manual evaluation of each IC was conducted to identify and remove ICs overlapping signal contamination from contracts or relaxes of blood vessel walls. The remaining ICs were assigned to one of the 28 distinct units closest to their center based on spatial arrangement and morphological characteristics. The extraction of fluorescence time-series signals for each unit was achieved by averaging pixel signals weighted spatially according to the assigned IC area (see Fig. S1).

Cortical activity with PLSR correction

The time series signals for each unit were standardized to cortical activity by z-score. In the analysis, PLSR was employed to eliminate behavior variables from the original cortical activity. After behavior analysis, the paw position, the swing pattern, and the walking speed during motorized track locomotion were extracted. In addition, the pupil area was calculated. These behavior variables were standardized by z-score and made available for PLSR correction. The PLSR analysis was executed using the MATLAB function "*plsregress*"[50]. Cortical activity was corrected for the dependent matrix ($n \times m$, n = observation, and m = number of units) and behavior variables were corrected in the independent matrix ($n \times p$, p = number of behavior variables). The observation revealed a specific pattern of cortical activity. PLSR calculated a latent as an output, defined as a behavior variables-driven activity that represented the covariance between an independent and a dependent data set following cross-validation and model evaluation. The proportion of variance in the dependent variable that was explained by the independent variables in the PLSR, represented as *R*-squared (R^2) (treadmill: 0.1323 ± 0.02263, wheel: 0.1537 ± 0.03285, disk: 0.1167 ± 0.01843, data are expressed as mean ± SEM). After the elimination of the latent activity from the original activity through linear correction, the residual activity was identified as internally driven cortical activity. Subsequently, we proceeded to categorize units that exhibited a statistically significant discrepancy between the activity of each behavioral period and the resting activity. The baseline-corrected activity exhibited a discernible modulation of the internally driven cortical activity of the unit. The cortical activity of each significant unit was represented by a homologous average of ipsilateral and contralateral activity in each behavioral period. *P*-values were calculated with a paired sample t-test using the MATLAB Statistics and Machine Learning Toolbox function "*ttest*" ($\alpha = 0.05$) and were adjusted for multiple comparisons with the Benjamini–Hochberg false discovery rate post-hoc correction method[51]. The PLSR regressions were executed with a total of one thousand possible permutations.

Cortical FC with PLSR correction

The signal-pairs connectivity between the original activity before PLSR of each unit was assessed using Pairwise Pearson correlation coefficients (r). The correlation value of a 1 s window (20 frames) was added in temporal order, with the correlation window shifted to a 0.25-s step (5 frames). Next, we obtained time-series of correlation matrices for each of the 378 pairs of units per mouse. For PLSR, the cortical FC was corrected into a dependent matrix ($n \times m$, n = observation, and m = number of pairs). The proportion of variance in the dependent variable that was explained by the independent variables in the PLSR, represented as R^2 (treadmill: 0.07584 ± 0.01351, wheel: 0.1460 ± 0.02442, disk: 0.1428 ± 0.03577, data are expressed as mean ± SEM). The observation entailed a solitary sliding window time in the cortical FC. Following PLSR correction, a statistical comparison was conducted between the signal correlation of each behavioral period (r_{signal}) and the resting correlation of rest (r_{rest}), with units exhibiting statistically

significant differences being identified. The calculation of internally driven cortical FC for each significant unit was derived from the difference between the r_{signal} and r_{rest} values. The cortical FC ($r_{signal} - r_{rest}$) of the units is represented by a homologous average of the ipsilateral and contralateral correlations of pairs in each behavioral period. All data presented in the figures were based on Pearson correlation coefficients, while statistical tests were performed on Fisher z-transformed correlation values to satisfy normality assumptions.

Relationship between cortical activity and FC after PLSR correction

The relationship indicated the similarity between cortical activity and FC of each unit during the behavioral period. We used the cortical activity and FC values from the same unit of individual animals within a track group as vectors. Next, the relationship between the cortical activity vector (a) and the FC vector (b) was calculated using the cosine similarity to ascertain the directional alignment between the two vectors. The cosine similarity is defined as the dot product divided by the product of the magnitudes of the two vectors. The relationship was calculated as follows:

$$relationship\ (a, b) = \frac{a \cdot b}{||a||\,||b||} \quad (1)$$

The relationship per unit is calculated as a single scalar value and the value of the relationship ranges from −1 to 1. The sign of the relationship indicates whether the variables are pointing in the same direction or in opposite directions. The score of the relationship reflects the strength of the relationship between activity and FC. As the score approaches 1 or −1, the relationship between the two variables becomes increasingly pronounced. As the score approaches 0, the relationship between the two variables becomes less pronounced.

Statistics and reproducibility

$N = 15$ biologically independent animals were used in the present studies. Statistical analysis was carried out with standard functions in Prism (GraphPad Software). Error bars in all cortical activity and FC figures represent the mean ± SEM and error bars in all figures of the gate analysis represent the mean ± SD. The number (n) of samples employed is indicated in figure legends. The differences of locomotion behaviors among three tracks were tested using one-way ANOVA, followed by Tukey's post-hoc test for multiple comparisons.

Reporting summary

Further information on research design is available in the Nature Portfolio Reporting Summary linked to this article.

Data availability

Quantitative data and source data supporting this study can be obtained at https://doi.org/10.5281/zenodo.18162257. Raw data files are available from K. Lee on reasonable request.

Code availability

The sICA can be downloaded from https://sccn.ucsd.edu/~arno/eeglab/auto/jader.html. The PLSR toolbox can be downloaded from https://kr.mathworks.com/products/statistics.html. The custom code for analysis supporting this study can be obtained at https://github.com/lch199912/Widefield_Code/tree/main/imaging_analysis.

Received: 31 July 2025; Accepted: 6 January 2026;
Published online: 13 January 2026

References

1. González-Rueda, A. et al. Kinetic features dictate sensorimotor alignment in the superior colliculus. *Nature* **631**, 378–385 (2024).
2. Parker, P. R. L., Brown, M. A., Smear, M. C. & Niell, C. M. Movement-related signals in sensory areas: roles in natural behavior. *Trends Neurosci.* **43**, 581–595 (2020).
3. Ayaz, A. et al. Layer-specific integration of locomotion and sensory information in mouse barrel cortex. *Nat. Commun.* **10**, 2585 (2019).
4. Heindorf, M., Arber, S. & Keller, G. B. Mouse motor cortex coordinates the behavioral response to unpredicted sensory feedback. *Neuron* **99**, 1040–1054.e1045 (2018).
5. Rao, R. P. N. A sensory–motor theory of the neocortex. *Nat. Neurosci.* **27**, 1221–1235 (2024).
6. Clancy, K. B., Orsolic, I. & Mrsic-Flogel, T. D. Locomotion-dependent remapping of distributed cortical networks. *Nat. Neurosci.* **22**, 778–786 (2019).
7. Arber, S. Motor circuits in action: specification, connectivity, and function. *Neuron* **74**, 975–989 (2012).
8. Omlor, W. et al. Context-dependent limb movement encoding in neuronal populations of motor cortex. *Nat. Commun.* **10**, 4812 (2019).
9. Cruz, K. G. et al. Cortical-subcortical interactions in goal-directed behavior. *Physiol. Rev.* **103**, 347–389 (2022).
10. Lu, L. et al. Control of locomotor speed, arousal, and hippocampal theta rhythms by the nucleus incertus. *Nat. Commun.* **11**, 262 (2020).
11. Melzer, S. et al. Distinct corticostriatal GABAergic neurons modulate striatal output neurons and motor activity. *Cell Rep.* **19**, 1045–1055 (2017).
12. Barthas, F. & Kwan, A. C. Secondary motor cortex: where 'sensory' meets 'motor' in the rodent frontal cortex. *Trends Neurosci.* **40**, 181–193 (2017).
13. Leinweber, M., Ward, D. R., Sobczak, J. M., Attinger, A. & Keller, G. B. A sensorimotor circuit in mouse cortex for visual flow predictions. *Neuron* **95**, 1420–1432.e1425 (2017).
14. West, S. L., Gerhart, M. L. & Ebner, T. J. Wide-field calcium imaging of cortical activation and functional connectivity in externally- and internally-driven locomotion. *Nat. Commun.* **15**, 7792 (2024).
15. Sun, G. et al. Neural representation of self-initiated locomotion in the secondary motor cortex of mice across different environmental contexts. *Commun. Biol.* **8**, 725 (2025).
16. Dana, H. et al. Thy1-GCaMP6 transgenic mice for neuronal population imaging in vivo. *PLoS ONE* **9**, e108697 (2014).
17. Kim, T. H. et al. Long-term optical access to an estimated one million neurons in the live mouse cortex. *Cell Rep.* **17**, 3385–3394 (2016).
18. Cardoso, J.-F. High-order contrasts for independent component analysis. *Neural Comput.* **11**, 157–192 (1999).
19. Wang, Q. et al. The Allen Mouse Brain Common Coordinate Framework: a 3D Reference Atlas. *Cell* **181**, 936–953.e920 (2020).
20. Vélez-Fort, M., Cossell, L., Porta, L., Clopath, C. & Margrie, T. W. Motor and vestibular signals in the visual cortex permit the separation of self versus externally generated visual motion. *Cell* **188**, 2175–2189.e2115 (2025).
21. Mao, D., Molina, L. A., Bonin, V. & McNaughton, B. L. Vision and locomotion combine to drive path integration sequences in mouse retrosplenial cortex. *Curr. Biol.* **30**, 1680–1688.e1684 (2020).
22. Dadarlat, M. C. & Stryker, M. P. Locomotion enhances neural encoding of visual stimuli in mouse V1. *J. Neurosci.* **37**, 3764 (2017).
23. West, S. L. et al. Wide-field calcium imaging of dynamic cortical networks during locomotion. *Cereb. Cortex* **32**, 2668–2687 (2021).
24. Aydın, Ç, Couto, J., Giugliano, M., Farrow, K. & Bonin, V. Locomotion modulates specific functional cell types in the mouse visual thalamus. *Nat. Commun.* **9**, 4882 (2018).
25. Vinck, M., Batista-Brito, R., Knoblich, U. & Cardin, J. A. Arousal and locomotion make distinct contributions to cortical activity patterns and visual encoding. *Neuron* **86**, 740–754 (2015).
26. McGinley, M. atthewJ., David, S. tephenV., McCormick & David, A. Cortical membrane potential signature of optimal states for sensory signal detection. *Neuron* **87**, 179–192 (2015).

27. Olson, J. M., Li, J. K., Montgomery, S. E. & Nitz, D. A. Secondary motor cortex transforms spatial information into planned action during navigation. *Curr. Biol.* **30**, 1845–1854.e1844 (2020).
28. Keshavarzi, S. et al. Multisensory coding of angular head velocity in the retrosplenial cortex. *Neuron* **110**, 532–543.e539 (2022).
29. Fischer, L. F., Mojica Soto-Albors, R., Buck, F. & Harnett, M. T. Representation of visual landmarks in retrosplenial cortex. *eLife* **9**, e51458 (2020).
30. Sun, H. et al. Conjunctive processing of spatial border and locomotion in retrosplenial cortex during spatial navigation. *J. Physiol.* **602**, 5017–5038 (2024).
31. Qadir, H. et al. The mouse claustrum synaptically connects cortical network motifs. *Cell Rep.* **41**, 111860 (2022).
32. Yamawaki, N., Radulovic, J. & Shepherd, G. M. G. A corticocortical circuit directly links retrosplenial cortex to M2 in the mouse. *J. Neurosci.* **36**, 9365 (2016).
33. Lazari, A. et al. The mouse motor system contains multiple premotor areas and partially follows human organizational principles. *Cell Rep.* **43**, 114191 (2024).
34. Reep, R. L. & Corwin, J. V. Topographic organization of the striatal and thalamic connections of rat medial agranular cortex. *Brain Res.* **841**, 43–52 (1999).
35. Allen, W. E. et al. Global representations of goal-directed behavior in distinct cell types of mouse neocortex. *Neuron* **94**, 891–907.e896 (2017).
36. Makino, H. et al. Transformation of cortex-wide emergent properties during motor learning. *Neuron* **94**, 880–890.e888 (2017).
37. Yoshida, E. et al. Whether or not to act is determined by distinct signals from motor thalamus and orbitofrontal cortex to secondary motor cortex. *Nat. Commun.* **16**, 3106 (2025).
38. Augusto, E. et al. Secondary motor cortex tracks decision value during the learning of a non-instructed task. *Cell Rep.* **44**, 115152 (2025).
39. Zamani Esfahlani, F. et al. High-amplitude cofluctuations in cortical activity drive functional connectivity. *Proc. Natl. Acad. Sci. USA* **117**, 28393–28401 (2020).
40. Sun, Q. et al. A whole-brain map of long-range inputs to GABAergic interneurons in the mouse medial prefrontal cortex. *Nat. Neurosci.* **22**, 1357–1370 (2019).
41. Holey, B. E. & Schneider, D. M. Sensation and expectation are embedded in mouse motor cortical activity. *Cell Rep.* **43**, 114396 (2024).
42. Schneider, D. M., Nelson, A. & Mooney, R. A synaptic and circuit basis for corollary discharge in the auditory cortex. *Nature* **513**, 189–194 (2014).
43. Gallero-Salas, Y. et al. F. Sensory and behavioral components of neocortical signal flow in discrimination tasks with short-term memory. *Neuron* **109**, 135–148 (2021).
44. Mohr, H. et al. Integration and segregation of large-scale brain networks during short-term task automatization. *Nat. Commun.* **7**, 13217 (2016).
45. Ghanbari, L. et al. Craniobot: A computer numerical controlled robot for cranial microsurgeries. *Sci. Rep.* **9**, 1023 (2019).
46. Warren, R. A. et al. A rapid whisker-based decision underlying skilled locomotion in mice. *eLife* **10**, e63596 (2021).
47. Aljovic, A. et al. A deep learning-based toolbox for Automated Limb Motion Analysis (ALMA) in murine models of neurological disorders. *Commun. Biol.* **5**, 131 (2022).
48. Mathis, A. et al. DeepLabCut: markerless pose estimation of user-defined body parts with deep learning. *Nat. Neurosci.* **21**, 1281–1289 (2018).
49. Syeda, A. et al. Facemap: a framework for modeling neural activity based on orofacial tracking. *Nat. Neurosci.* **27**, 187–195 (2024).
50. de Jong, S. SIMPLS: an alternative approach to partial least squares regression. *Chemom. Intell. Lab. Syst.* **18**, 251–263 (1993).
51. Genovese, C. R., Lazar, N. A. & Nichols, T. Thresholding of statistical maps in functional neuroimaging using the false discovery rate. *NeuroImage* **15**, 870–878 (2002).

Acknowledgements

We thank S.L. West and T.J. Ebner for analytical assistance with widefield imaging. This work was supported in part by the National Research Foundation of Korea (NRF) grant funded by the Korea government (MSIT) (RS-2021-NR065783, RS-2025-16903034), in part by the "DGIST intramural grant" (25-IRJoint-03, 25-HRHR-02).

Author contributions

Study conception and design: K.L., G.L., H.S., C.H.L.; Experiments performing and data collection: C.H.L.; Visualization and data analysis: K.L., C.H.L., G.L., H.S.; Funding acquisition: K.L.; Project administration: K.L.; Supervision: K.L.; Results were discussed and interpreted by: K.L., G.L., H.S., C.H.L.; Writing—original draft: K.L., C.H.L., G.L., H.S.; Writing—review and editing: K.L., G.L., H.S.

Competing interests

The authors declare no competing interests.

Additional information

Supplementary information The online version contains supplementary material available at https://doi.org/10.1038/s42003-026-09541-x.

Correspondence and requests for materials should be addressed to Kwang Lee.

Peer review information *Communications Biology* thanks the anonymous reviewers for their contribution to the peer review of this work. Primary handling editor: Jasmine Pan.